Initial stages of oxidation of Si(111) with condensed O_2 and N_2O at 20 K

J. M. Seo, S. E. Harvey, Y. Chen, and J. H. Weaver
Department of Materials Science and Chemical Engineering, University of Minnesota, Minneapolis, Minnesota 55455
(Received 26 December 1990)

The oxidation induced by soft-x-ray illumination of condensed multilayers of O_2 and N_2O on cleaved Si(111) at 20 K has been investigated with high-resolution core-level spectroscopy. The results for O_2/Si(111) show that a SiO_2 phase is produced by illumination with as few as 4.3×10^{13} photons cm^{-2} of energy 130 eV. This Si^{4+} oxide is characterized by a Si $2p$ binding energy that is shifted 3.4 eV relative to bulk Si, and its effective thickness increases with illumination. Intermediate oxides having Si^{1+}, Si^{2+}, and Si^{3+} bonding configurations are also observed, and their total thickness also increases. The enhanced formation of these intermediate oxides is due primarily to the growth of Si^{3+} bonding configurations throughout the SiO_2 layer. Exposure of the oxidized Si surface to white light from the synchrotron-radiation source or annealing to 300 K produces structural changes as the SiO_2 layer thickens at the expense of the intermediate oxides. Hence, the defectlike Si^{3+} configuration converts to a SiO_2 configuration and a sharper interface develops. Studies of N_2O/Si(111) interactions during photon irradiation show that the initial oxidation rate is slower than with O_2. After more extended illumination, the oxidation rate with N_2O approximates that with O_2 as N_2O molecules are dissociated. The intermediate oxide formed with N_2O is thicker than with O_2, and extended growth of the intermediate oxide reflects the formation of both Si^{2+} and Si^{3+}. From these O_2 and N_2O results, we conclude that the oxidation rate for the submonolayer oxide is determined mainly by the availability of surface reaction sites and the cross section for electron capture by the condensed species. Further oxide growth is also limited by the existing oxide layer through which atomic oxygen must diffuse in order to react at the interface.

INTRODUCTION

The structural and chemical properties of the SiO_2-Si interface have been investigated extensively (see, for example, Refs. 1–6), and the electrical properties have been attributed to the fact that the interface is ~5 Å wide.[7] Photoemission studies of the oxidation processes for Si(111) have indicated that the SiO_2-Si boundary layer consists of Si^{1+}, Si^{2+}, and Si^{3+} bonding configurations, where Si^{n+} denotes coordination with n oxygen atoms. These initial stages of oxidation for Si(111) offer insight into the corresponding reaction processes at the buried SiO_2-Si interface where Si^{n+} bonding configurations are established as O diffusion through the oxide barrier.

In this paper we examine surface oxidation for Si(111) at 20 K and effects of probe beams as they influence oxidation.[8,9] In these studies, condensed layers of O_2 and N_2O provide the oxygen needed for reaction and, as we will show, the photon beam used in the measurements induces the reaction. Thus, the semiconductor surface is oxidized by the sequential processes of photoinduced secondary electron attachment to the overlaying species and molecular dissociation, namely $O_2\rightarrow O_2^-\rightarrow O+O^-$ and $N_2O\rightarrow N_2O^-\rightarrow N_2+O^-$. We emphasize several important points that can be derived from these photoemission studies. First, oxidation at 20 K yields chemical shifts of the Si $2p$ binding energies that are determined primarily by the local oxygen coordination number Si^{n+}. Annealing to 300 K after oxidation at 20 K relaxes the kinetic constraints on the local structure, and this is reflected by changes in the Si $2p$ binding energy in SiO_2 (from ~3.4 eV to ~3.9 eV relative to the bulk Si $2p$ core level). Illumination with the zeroth-order synchrotron-radiation beam at 20 K produces similar binding-energy shifts as achieved by thermal processing. These SiO_2 structural changes therefore reflect both thermal and athermal processes. Second, these results show that the intensity of the Si^{3+} species increases in parallel with the Si^{4+} species, even after the Si^{1+} and Si^{2+} species have ceased to grow.[2,4,6] However, the SiO_2 phase grows at the expense of the Si^{3+} species after annealing to 300 K so that a relatively sharp interfacial layer is produced. This indicates that the anomalously strong Si^{3+} emission at 20 K is due to extended Si^{3+} bonding in the SiO_2 layer. We conclude that the oxide formed at 20 K involves less ordered SiO_2 compared with thermally grown oxides and that the more extended intermediate oxide consists mainly of Si^{3+} species. Annealing induces the conversion of the intermediate oxide to SiO_2 and the formation of a more ordered SiO_2.

Third, reaction of Si(111) with N_2O at 20 K reflects a slower initial oxidation rate than with O_2. This is shown by the fact that illumination with 4.3×10^{13} photons cm^{-2} produced an oxide layer that was 2.5 Å thick for 2 L of O_2 while illumination with 1×10^{14} photons cm^{-2} produced a layer that was only 0.5 Å thick for 4 L of N_2O (the amount of condensed gas was chosen to provide the same amount of available oxygen).

Despite these differences during the early reaction stages, the oxidizers showed equivalent oxidation rates for extended photon exposures. This suggests that N_2O is much less efficient in supplying O compared to O_2 at the first-monolayer-reaction regime. Once started, however, the factors governing oxidation were the same as for O_2. These factors reflect the amount of O available and the thickness of the oxide since that layer acts as a diffusion barrier. Finally, the interfacial oxide formed with N_2O is broader than that formed with O_2, indicating that the surface is oxidized more evenly with O_2 than N_2O at 20 K.

EXPERIMENT

The photoemission experiments were conducted at the Wisconsin Synchrotron Radiation Center. Photoelectrons were collected with an angle-integrated double-pass cylindrical-mirror analyzer. The Si $2p$ core-level spectra were analyzed with a least-squares-minimization routine that made it possible to decompose the spectra into components and to determine the intensities of each.[10] Phosphorus-doped Si samples (doped at 1×10^{15} cm^{-3}) were cleaved at 300 K at pressures of $\sim3\times10^{-11}$ Torr to produce mirrorlike (111) surfaces. The samples were bonded to the cold head of a closed-cycle helium refrigerator with Ga solder and were cooled to 20 K (±5 K), as described elsewhere.[11] Reference photoemission spectra were acquired prior to O_2 or N_2O exposure. These spectra emphasized the valence bands ($h\nu=65$ eV) and the Si $2p$ core levels, where the latter core-level energy-distribution curves (EDC's) were obtained using photon energies of 130 and 115 eV to change the surface sensitivity. O $1s$ and N $1s$ core-level spectra were not acquired because of the modest resolution of the monochromator at energies of 450 to 600 eV. The cleaved samples were exposed to O_2 or N_2O at 5×10^{-8} Torr. The valence-band features were used to monitor the chemical state and determine the amount of molecular species on the surface. The O_2 experiments were conducted as a function of exposure from 0.5 to 20 L, where 1 L$=10^{-6}$ Torr sec. The photon flux used to induce surface reaction was estimated by measuring the total electron yield from a 90% transparent W mesh permanently installed between the exit slit of the monochromator and the sample surface. A photon shutter was used to interrupt the synchrotron-radiation beam, and the intensity of the beam incident on the sample was controlled by adjusting the monochromator slits. The total exposure of the sample was the product of the exposure duration and average yield from the W mesh during that time. The yield of W was calibrated by comparison with the known yield of a Au standard. After the reaction saturated for irradiation with 130-eV photons for 20 L O_2 exposure, the sample was exposed to the zeroth-order beam transmitted by the beamline. This consumed any remaining O_2 on the surface. Photoemission spectra were then acquired to characterize the resulting surface bonding configurations. Finally, the sample was warmed to 300 K to assess changes related to surface oxides and the changes in kinetic constraints. Similar experimental procedures were followed for condensed layers of N_2O on Si(111). In this case, the gas dosage was adjusted to condense the same amount of oxygen so that direct comparison could be made.

Photoinduced oxidation of condensed O_2 on Si(111)

Low-coverage regime: 0.5–2 L of O_2

In the low-coverage regime, it is possible to monitor the early stages of reaction during soft-x-ray illumination based on changes in the valence band and Si $2p$ core-level EDC's. Figure 1(a) shows the angle-integrated valence-band spectrum for clean cleaved Si(111) where structure is evident at 1.5, 3.5, and 8 eV. Exposure to 0.5 L O_2 at 20 K produced the $1\pi_g$, $1\pi_u$, and $3\sigma_g$ molecular orbital features of O_2, as identified. Subsequent irradiation with 130-eV photons produced a broadening of the O_2 features. After a total exposure equal to 3.9×10^{15} photons cm^{-2} of 130-eV photons, the O_2 molecular orbital features were replaced by the broad Si—O bonding structures at ~6 and ~11 eV. Conversion from physisorbed O_2 to the reaction products required photon irradiation and was not thermally activated. This was easily demonstrated in another experiment in which O_2 was condensed in the dark and data acquisition was delayed for 1 h. There were no changes in the valence-band spectra that would indicate spontaneous reaction of O_2 with Si(111) at 20 K.

Figure 1(b) shows Si $2p$ core-level EDC's for O_2 exposures up to 2 L for different levels of illumination by 130-eV photons. To obtain these spectra, the surface was first exposed to 0.5 L O_2 and 3.9×10^{15} photons cm^2 [as in Fig. 1(a)], then exposed to another 0.5 L O_2 and illuminated with an additional 3.2×10^{16} photons cm^{-2}, then finally exposed to another 1 L O_2 and another 8.8×10^{14} photons cm^{-2}. Changes due to reaction are highlighted by superimposing the clean surface spectrum on each of the other EDC's, with normalization to the intensity of the maximum emission. Analysis of these spectra gives the emission intensities of the bulk component, the surface-shifted component, and the total oxide component. For the conditions shown, the oxide peaks represented 11%, 24%, and 34% of the total emission, respectively. (We use relative emission intensities to eliminate artifacts due to attenuation by any residual O_2.) Line-shape analysis shows the persistence of the surface-shifted Si $2p$ component after 1 L O_2 exposure and illumination because the surface layer was not fully consumed (the surface-shifted component was reduced to 43% of its starting value, a change that would be more apparent if the spectra were normalized to the bulk Si $2p_{3/2}$ component rather than the peak height). Inspection also shows that the oxide emission was derived from more than a single species, with bonding likely to range from Si^{1+} to Si^{4+}. During these early stages of reaction with condensed O_2, oxide growth was heterogeneous in character and not simply layer by layer.

The results of Fig. 1(b) show extensive reaction but the valence-band spectra under the conditions corresponding to the uppermost Si $2p$ EDC showed the persistence of

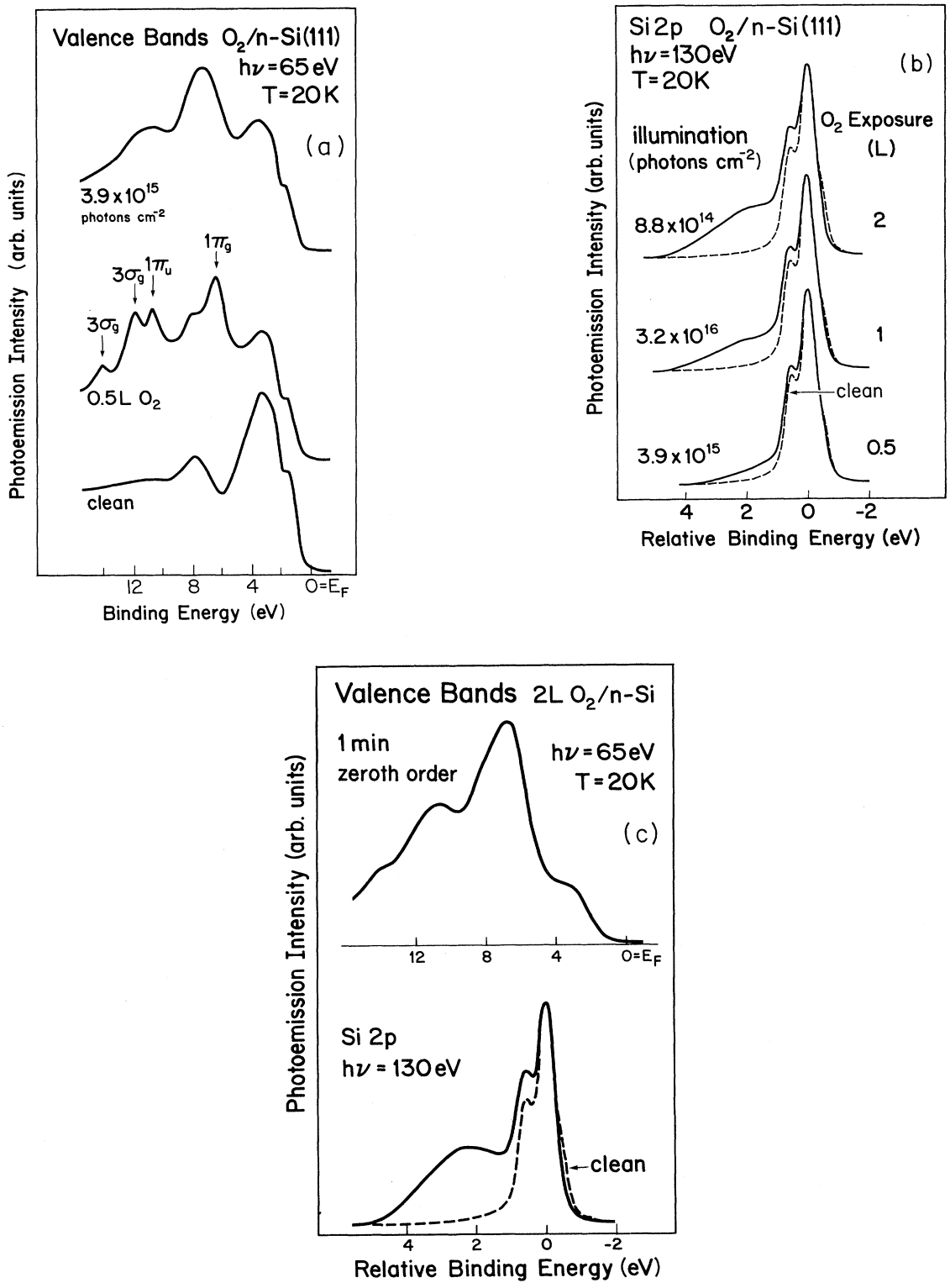

FIG. 1. Valence band and Si 2*p* core-level EDC's for *n*-Si (111) at 20 K after exposure to O_2 and illumination with $h\nu = 130$ eV. (a) Valence bands for the clean Si(111) surface before and after exposure to 0.5 L O_2 (middle) and then 3.9×10^{15} photons cm^{-2} (top). Four molecular O_2 levels appear in addition to substrate features at 3.4 and 8 eV, but these broaden as Si—O derived structure appears near 7.5 and 11 eV. (b) Si 2*p* spectra for clean Si(111) (dashed) and for representative oxygen exposures and photon irradiation. (c) Si 2*p* and valence-band spectra showing the effect of irradiation with zeroth-order radiation for the surface represented by the top EDC of (b).

molecular O_2. To enhance consumption of this residual O_2, we exposed the surface to the zeroth-order beam transmitted by the beamline for 1 min. Under these conditions, the surface was exposed to photons of energy 2–1200 eV. Figure 1(c) shows the Si 2*p* and valence-band emission acquired thereafter. Comparison with Figs. 1(a) and 1(b) reveals additional conversion to Si—O bonding. Indeed, under these conditions the total oxide emission amounted to 43% of the overall Si 2*p* emission, and there was no evidence of a surface-shifted Si 2*p* component. It is noteworthy that the photoenhanced oxidation rate slowed after the first layer of oxide had formed, an effect that can be understood by noting that the oxide acts as a diffusion barrier and that the proximity of O_2 to the surface is reduced.

High-coverage regime: 2–20 L of O_2

Figure 2 shows Si 2*p* core-level EDC's for successive exposures to O_2 and irradiation with 130-eV photons. The surface was first exposed to 2 L O_2 and then allowed to react fully during photon illumination, a condition reached by 8.2×10^{15} photons cm^{-2}. Additional O_2 exposures gave totals of 5 and 10 L O_2 with each exposed to previously reacted surfaces. The photon irradiation levels were reset to zero after each O_2 exposure. The spectra have been background subtracted, and the contributions from the different oxidation states have been estimated based on a least-squares-minimization routine.[10] For 2 L O_2 exposure, the SiO_2 or Si^{4+} phase was produced by illumination by as few as 4.3×10^{13} photons cm^{-2} (not shown). Analysis reveals that the relative intensity ratio $Si^{1+}/(Si^{1+}+Si\ bulk)$ increased from 0.23 to 0.29 for photon irradiation from 4.3×10^{13} to 8.2×10^{15} photons cm^{-2}. That ratio did not change during subsequent oxidation, in agreement with results obtained during elevated temperature oxidation.[4] The results of Fig. 2 also show that the intermediate oxide intensities scaled as $I(Si^{1+})>I(Si^{3+})>I(Si^{2+})$ for 2 L exposure. Note that Si^{1+} and Si^{3+} bonding configurations are preferred over Si^{2+} geometries at the ideal interface between Si(111) and SiO_2. The observed mixture of Si^{1+} and Si^{3+} indicates that the interface is broader than a single layer and a small portion of Si^{2+} appears at the boundary of these layers.

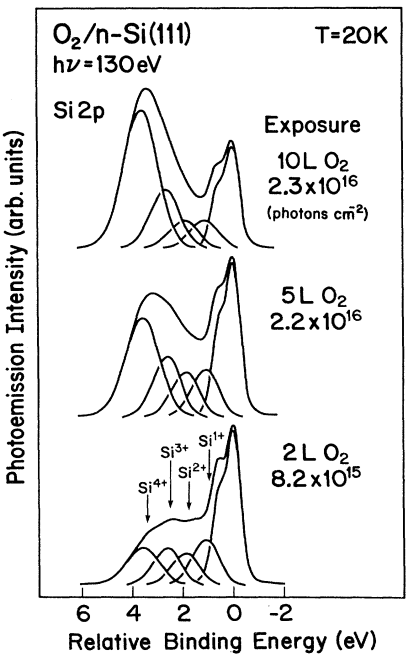

FIG. 2. Si 2*p* core-level EDC spectra for Si(111) held at 20 K after O_2 exposures from 2 to 10 L. From the bottom panel, four reacted oxide peaks are evident at 0.95, 1.8, 2.5, and 3.4 eV. The middle panel shows that only Si^{3+} and Si^{4+} grow when the surface represented by the bottom EDC is exposed to an additional 3 L O_2 and photon exposure of 2.2×10^{16} photons cm^{-2}. The top panel shows the continued growth of Si^{3+} and Si^{4+} with 5 L O_2 of additional exposure and photon exposure of 2.3×10^{16} photons cm^{-2}.

Insight into the structure and bonding configurations for the Si oxides formed at 20 K can be gained by considering the relative binding-energy shifts from the bulk, namely 1.0, 1.8, and 2.5 eV for Si^{1+}, Si^{2+}, and Si^{3+}, respectively. These binding energies do not change during enhanced oxidation (Fig. 2). However, comparison of the shift of the Si^{4+} species (i.e., SiO_2) shows that it is ~0.5 eV less than that observed when SiO_2 was formed at elevated temperatures (3.4 eV versus 3.9 eV). Grunthaner *et al.*[12] have shown that the Si—O—Si bond angle is related to the binding energy and that the lower binding energy is associated with the smaller angle. This suggests that SiO_2-like structures formed at 20 K have a smaller Si—O—Si bond angle than those formed at elevated temperatures,[4,13] presumably because of a less ordered structure for growth at low temperature.

Figure 2 shows that oxide growth is accompanied by significant changes in relative intensities for the different components when 3 L O_2 is condensed on the reacted and illuminated surface. In particular, the intensity of Si^{2+} emission reaches that of Si^{1+} and the intensities of both Si^{3+} and Si^{4+} increase to give an intensity ratio for 5 L total O_2 of $I(Si^{1+}):I(Si^{2+}):I(Si^{3+})=1:1:1.3$. For the more extended reactions produced with total exposures of 10 L (top Fig. 2) and 20 L (not shown) and irradiation, the corresponding values were 1:1:2.1 and 1:0.9:2.6. This continuous increase in the Si^{3+} component at low temperature paralleled that observed in elevated temperature oxidation,[2,3,8] and the steady increase in the Si^{4+} has also been reported.

Himpsel *et al.*[4] recently concluded that the Si 2*p* photoionization cross sections for $h\nu=130$ eV scaled as $I(Si^{1+}):I(Si^{2+}):I(Si^{3+}):I(Si^{4+})=1:1.1:1.7:2.2$ based on their studies of oxidation at 300 K. The ratio of 1.7 for Si^{3+} to Si^{1+} was used to argue that Si^{3+} could grow during oxidation in a manner that did not reflect extended defect formation in the SiO_2 layer. Our measurements with photon energies of 115 eV showed that the ratio of Si^{3+} to Si^{1+} is 1 for 5 L, 1.8 for 10 L, and 2.6 for 20 L. This compares to 1.3 for 5 L, 2.1 for 10 L, and 2.6 for 20 L for $h\nu=130$ eV. Hence, the increase in the Si^{3+} emis-

sion for the thicker oxide formed from 20 L exposure and irradiation does not arise only from differences in the photoionization cross section but rather that it reveals differences in the growth of Si^{3+} at 20 K. From the reduction of Si^{3+} relative to Si^{1+} for 5 and 10 L in the bulk-sensitive spectra ($h\nu=115$ eV), we conclude that the Si^{3+} species are closer to the vacuum surface than are Si^{1+} and Si^{2+}. For the oxide formed with 20 L, the Si^{3+} to Si^{1+} ratio approaches the value derived from the surface-sensitive spectra. This indicates that bonding states are mixed with Si^{4+} and Si^{1+} and Si^{2+} configurations.

In photoenhanced Si oxidation with condensed O_2, the dynamics of the process are complex and, while photons initiate the process, there is no simple functional form that relates the oxide thickness to the photon exposure. Indeed, oxidation rates reflect the energy distribution of the excited electrons in the substrate, the cross section for electron capture by O_2 to form reactive O_2^-, the diffusion of atomic oxygen through any surface barrier (e.g., the condensed overlayer or the oxide), and the amount of oxygen on the surface. It is, therefore, instructive to relate the empirical variations in the oxide species to the photon exposure so as to better understand the changing roles of these processes during growth.

The effective oxide thicknesses can be estimated from their intensity ratios. These intensity ratios provide more reliable information about oxide thicknesses than the absolute intensities, because the thicknesses of the condensed molecular layers vary and they attenuate the emission from beneath during low-temperature photoinduced oxidation. If we assume that only a single phase SiO_2 forms with thickness d, then the substrate intensity I_s is

$$I_s = I_{0s}\exp\left[-\frac{d}{\lambda}\right], \tag{1}$$

where I_{0s} is the initial intensity from the substrate and λ is the attenuation length in the SiO_2 overlayer. Then

$$d=\lambda\ln\left[\frac{I_{0s}}{I_s}\right]=\lambda\ln\left[\frac{1}{\left[\frac{I_s}{I_s+I_{SiO_2}}\right]}\frac{1}{\left[\frac{I_s+I_{SiO_2}}{I_{0s}}\right]}\right], \tag{2}$$

where I_{SiO_2} is the intensity of the SiO_2. The second factor in the brackets can be rewritten as

$$\frac{I_s+I_{SiO_2}}{I_{0s}}=\frac{I_s}{I_{0s}}+\frac{1}{I_{0s}}\frac{I\infty}{\lambda}\int_0^d\exp\left[\frac{-z}{\lambda}\right]dz$$
$$=\frac{I_s}{I_{0s}}+\frac{I_\infty}{I_{0s}}\left[1-\exp\left[-\frac{d}{\lambda}\right]\right], \tag{3}$$

where I_∞ is the intensity from an infinitely thick SiO_2 layer. Substituting Eq. (3) into Eq. (2) gives

$$d=\lambda\ln\left[\frac{1+a\alpha-a}{a\alpha}\right], \tag{4}$$

where $a\equiv I_s/(I_s+I_{SiO_2})$ and $\alpha\equiv I_\infty/I_{0s}$. Note that a is determined experimentally. The parameter α merely reflects the photoemission intensity ratio between SiO_2 and Si as determined by the photoionization cross section and the density of Si atoms in each material.

Equation (4) gives the thickness of a homogeneous SiO_2 layer based on the measured relative intensity of SiO_2 and the substrate. As a simple approximation, one can choose to group the emission intensity of the intermediate oxides with the substrate or the SiO_2 overlayer. In the former case, d is the thickness of the SiO_2 layer. In the latter, it is the total thickness of the oxide layer. The difference between these values will be the thickness of the intermediate oxides. To approximately include oxide inhomogeneity in each layer, we adjust the parameters α and λ. For calculations of the total oxide thickness, λ is taken as the weighted average of the values for the different oxides, and the weights reflect the amounts of each oxide species as determined by their photoemission intensities. We used values of the attenuation lengths for Si^{0+}, Si^{1+}, Si^{2+}, Si^{3+}, and Si^{4+} as 3.3, 4.25, 5.2, 6.15, and 7.1 Å, respectively. The parameter α is also adjusted to account for differences in photoionization cross section and the density of Si atoms. The values of α for Si^{0+}, Si^{1+}, Si^{2+}, Si^{3+}, and Si^{4+} are 1, 1, 1.1, 1.7, and 2.2, respectively. As an example of calculating the thickness of homogeneous SiO_2, λ is simply the mean free path in SiO_2, 7.1 Å, and α is the average of the values above with weighting factors that reflect the amount of each oxide determined from the relative photoemission intensities.

Figure 3 shows how the oxide thicknesses evolve as a function of photon exposure, calculated with Eq. (4) and the parameter adjustment discussed above. The upper panel shows the total oxide (SiO_2+SiO_x) and the lower panel shows the SiO_2 component. The difference between the upper and lower panels then gives the SiO_x thickness. For 2 L O_2 exposure of Si(111) at 20 K, irradiation by 4.3×10^{13} photons cm^{-2} (the first data point) is sufficient to yield ~80% of the SiO_x that can be formed, based on values after prolonged irradiation. The number of O atoms in the oxide layer formed by illumination with 2.2×10^{14} photons cm^{-2} is estimated to be 1.1×10^{15} cm^{-2}. The extent of oxidation cannot be accounted for if it is assumed that oxidation is triggered only by direct photoinduced O_2 dissociation at the surface (i.e., O_2 dissociation following photoabsorption by the O_2 molecule). Instead, oxidation at 20 K for condensed O_2 on Si(111) reflects the capture of low-energy electrons excited following photoillumination of the substrate. These results are then qualitatively consistent with those discussed previously for photoenhanced oxidation of III-V semiconductor surfaces.[9] Electron capture by molecular O_2 in contact with the substrate readily yields Si oxidation, as is evident from the observed rapid oxidation [the total oxide thickness increased 2.5 Å for (2 L O_2)/Si(111) following illumination with as few as 4.3×10^{13} photons cm^{-2}]. In contrast, oxidation is slowed thereafter because the formed oxide barrier isolates the activated O_2^- species from the Si surface and the amount of O_2 is reduced on the surface. When the oxygen exposures are increased by

incremental dosages to 5, 10, and 20 L, larger photon exposures are needed to reach a state of saturated oxidation. In this region, the effect of oxygen photodesorption also becomes important.[9]

The results summarized in the upper panel of Fig. 3 show that the total oxide layer increases after each increment in O_2 exposure, with amounts of 1.2, 0.7, and 0.2 Å for illumination of 5×10^{14} photons cm^{-2} exposures for totals of 5, 10, and 20 L O_2, respectively. In each case, the oxide increment diminishes although the amount of O_2 exposure increases. This indicates that the oxide growth is controlled by the thickness of the existing oxide rather than simply the availability of O_2 for oxides thicker than ~3 Å.

For Si oxidation, the total thickness increases when diffusing O atoms arrive at the Si substrate. Because of kinetic constraints on oxygen movement, the oxides with the highest O coordination are formed closer to the vacuum surface (the source of oxygen) and the proportion of SiO_2 increases for the thicker oxides, as is evident by comparing the incremental changes in SiO_2 and SiO_x in Fig. 3. Moreover, analysis of line-shape changes during continued oxidation shows that the growth of the intermediate oxides (SiO_x of Fig. 3) occurs in large measure because of enhanced formation of Si^{3+} states (although the increase slows as the oxide thickens). This is in contrast to the behavior for oxidation at elevated temperatures (300–1200 K).[2,4,6] We also note that the binding energy of SiO_2 relative to bulk Si appears shifted only 3.4 eV (Fig. 2) compared to 3.9–4.5 eV for high-temperature growth of SiO_2. This indicates a less ordered form of SiO_2 for growth at 20 K. It is likely that this low-temperature structure can host more defectlike Si^{3+} compared to the well-ordered SiO_2.

The results of Fig. 4 emphasize the effects of zeroth-order irradiation (middle) and annealing (top) of an oxide layer formed at 20 K (bottom). In this case, the oxidized surface represented by the top EDC of Fig. 2 was exposed to 10 L O_2 and then illuminated by 2.4×10^{16} photons cm^{-2} of energy 130 eV. The valence bands for this surface showed residual molecular oxygen because the photon exposure was not sufficient to induce complete reaction with the substrate or complete desorption (see also Fig. 3). Comparison to the top spectrum of Fig. 2 shows additional growth of Si^{4+} and Si^{3+}. While the intensity ratio of Si^{3+} to Si^{1+} increased from 2.1 to 2.6, the relative intensity of Si^{1+} or Si^{2+} to the bulk emission did not change. This is consistent with the discussion above that Si atoms with Si^{1+} and Si^{2+} bonding were distributed near the interface, while those with Si^{3+} character were extended throughout the SiO_2 layer when the ox-

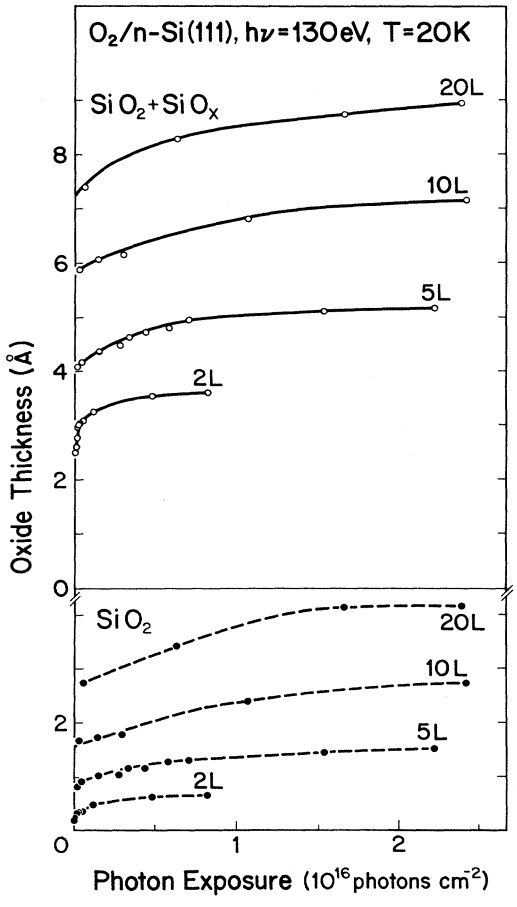

FIG. 3. Estimated thickness of the oxide layers as a function of photon exposure. The bottom panel shows the behavior for SiO_2 while the top shows that for the total oxide. The photon flux is reset to zero after each successive O_2 exposure. As few as 4.3×10^{13} photons cm^{-2} were able to produce an oxide 2.5 Å thick.

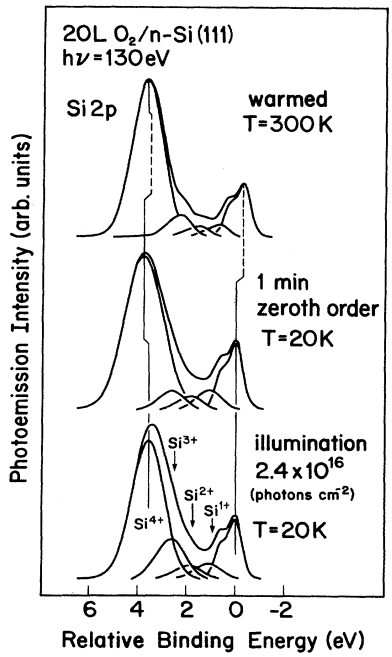

FIG. 4. Variation in the oxide layer formed from 20 L O_2 and illumination by 2.4×10^{16} photons cm^{-2} (bottom panel) after illumination by zeroth-order light and then annealing to 300 K.

ygen content of the surface was high. The EDC obtained after zeroth-order illumination (2–1200 eV) for 1 min showed an increase in the thickness of the SiO_2-like oxide of ~1 Å, corresponding to a 10% increase in relative intensity. The relative Si^{3+} intensity also decreased by 10%, but the total oxide thickness did not change. Hence, Si^{3+} species in the SiO_2 layer were converted to SiO_2 as the supply of O from the remaining O_2 was increased during irradiation. In addition, the Si^{4+} peak shifted 200 meV to higher binding energy. This change was due to chemical shifts rather than changes in band bending, because the substrate peak position did not change. We associate it with a structural change such that the Si—O—Si bond angles increased and the distance between Si atoms in Si—O—Si increased.[12,13] The conversion of the defectlike Si^{+3} bonding into SiO_2 structures and changes in the SiO_2 indicate the formation of a more nearly ideal SiO_2 layer.

The Si 2*p* core-level EDC shown at the top of Fig. 4 was obtained after the oxidized surface was warmed to 300 K to eliminate the nonequilibrium surface photovoltaic effect.[14] Whereas the bulk Si 2*p* emission and the intermediate oxides shifted 300 meV to lower binding energy upon warming, the Si^{4+} species shifted only 200 meV to produce a net increase in separation between Si^{4+} and bulk Si. Hence, annealing to 300 K induced oxide reordering due to the redistribution of O atoms among the oxide species. The results of Fig. 4 show that the intensity of Si^{3+} increased at the expense of Si^{2+} and Si^{1+} bonding, and the intensity ratio of Si^{1+} to Si^{2+} to Si^{3+} was 1:0.9:1.8. Hence the stable interfacial oxygen coordinations were Si^{1+} or Si^{3+}, but a non-negligible amount of Si^{2+} persisted. We estimate that the interface between Si and the oxide warmed to 300 K extended over at least two layers (~4 Å). This interface relieves strain between SiO_2 and the substrate while maintaining the bonding network of the Si substrate during oxygen insertion at the interface.

Photoinduced oxidation of condensed N_2O on Si(111) at 20 K

Studies of N_2O reaction with Si(111) were undertaken to compare oxidation rates and products to those for O_2 condensed at 20 K. For these studies, the N_2O exposures were adjusted to provide the same number of oxygen atoms as in the O_2 studies above. The fact that the initial oxidation rate with N_2O was at least one order of magnitude slower than with O_2 (as will be shown) enabled the acquisition of data with better statistics, and this resulted in better line-shape fitting in the low-coverage regime. For N_2O it was possible to observe the initial appearance of the intermediate oxides, something that was nearly impossible for O_2/Si(111).

Figure 5 shows Si 2*p* core-level EDC's for 4, 10, and 20 L N_2O exposures at 20 K following illumination by 130-eV photons in the amounts given. As above, the first exposure to 4 L was irradiated until reaction was saturated, then more N_2O was condensed and so forth. After 4 L exposure and relatively modest illumination, the EDC's showed Si^{1+}, Si^{2+}, and Si^{3+} reacted components in addition to the surface-shifted and bulk components. The

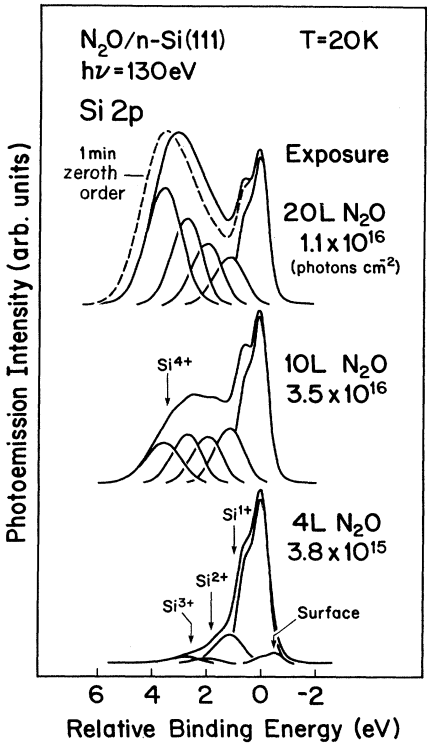

FIG. 5. Si 2*p* core-level EDC's spectra for Si held at 20 K after N_2O exposure and photon irradiation. The bottom panel shows three intermediate oxides and a surface-shifted component, but there was no evidence of SiO_2 formation. SiO_2 appears after additional N_2O exposure and illumination. The dashed line shows the effect of zeroth-order light.

most interesting point is that the intensities of the intermediate oxides appeared in the order of Si^{1+}, Si^{3+}, Si^{2+} rather than Si^{1+}, Si^{2+}, Si^{3+}. In the literature, it is usually accepted that the stable Si^{1+} state is due to O insertion into the backbonds of Si rather than chemisorption involving Si dangling bonds.[5] If the next occupation site of O were another backbond of the same Si atom, then Si^{2+} would appear prior to Si^{3+}. However, we observed that Si^3 appeared prior to Si^{2+}, indicating that the O site after the initial insertion into the backbond involved Si dangling bonds. The double bond for a single O atom at the dangling-bond site of Si with a single backbond induced the Si^{3+} state. This Si^{3+} configuration is a transient state that exists during initial oxidation, but it is not the same as the Si^{3+} structure in the interfacial layer. The results for 4 L N_2O exposure also show a reduction in the surface-shifted component commensurate with an increase in the Si oxides. The Si^{4+} bonding is evident at about the stage when the surface component disappears, after irradiation by 1.6×10^{16} photons cm^{-2}.

The middle EDC of Fig. 5 shows Si 2*p* emission obtained after 6 L of N_2O were condensed on the oxidized surface. Analysis shows Si oxides that extend from Si^{1+} to Si^{4+}, with energies of 1.0, 1.8, 2.6, and 3.4 eV. These energies agree with those obtained by oxidation with O_2. Analysis also shows that the Si^{1+} intensity saturates when the ratio of Si^{1+} to (Si bulk + Si^{1+}) reaches 0.3.

With increasing N_2O exposure, the Si^{2+},Si^{3+}, and Si^{4+} components increase, as shown in the top EDC of Fig. 5 (solid line). The continued growth of the Si^{2+} component is in contrast to oxidation using O_2 (Fig. 2). This indicates a wider interface because the ideal abrupt interface would have Si^{1+} or Si^{3+} states at the (111) substrate. We note that a similar anomalous growth of the intermediate oxide was also observed during oxidation of GaAs with condensed N_2O.[15]

Figure 5 also shows a Si $2p$ EDC obtained after exposure of the reacted surface to zeroth order for 1 min to consume or desorb any remaining N_2O (dashed line at top). With this enhanced reaction, the Si^{4+} energy increased by 0.13 eV, and the SiO_2 intensity increased at the expense of the intermediate oxide. While the total oxide thickness did not change, the increase of SiO_2 at the expense of lower-O coordination species indicates the increase of O in the oxide layer following N_2O dissociation by the zeroth-order beam. The conversion from lower to higher oxidation states reflects an ordering within the oxide layer analogous to that shown in the middle of Fig. 4 for O_2/Si(111).

Equation (4) makes it possible to estimate the thicknesses of SiO_2 and the total oxide so that the reaction rates can be compared with those for O_2. Figure 6 shows the increase in the oxide thickness as a function of 130-eV photon exposure. For 4 L N_2O, the total thickness of the intermediate oxide was 1.6 Å after 1.5×10^{16} photons cm^{-2} irradiation and the SiO_2 component had not yet appeared (Fig. 5). With additional 6 L N_2O exposure (total 10 L N_2O), the total thickness increased to 4 Å with 2×10^{16} photons cm^{-2} irradiation (85% of the thickness was due to the intermediate oxide, as can be seen from the difference between the solid line for total oxide and the dashed line for SiO_2). Oxidation continued after an additional 10 L N_2O exposure (total 20 L N_2O), giving a total oxide of 6.4 Å after 1.1×10^{16} photons cm^{-2} irradiation. Finally, after zeroth-order beam illumination, the SiO_2 thickness increased by $\sim$1 Å, while the intermediate oxide decreased by the same amount. We note also that an initial irradiation with 1×10^{14} photons cm^{-2} for the surface exposed to 4 L N_2O produced only the Si^{1+} component. At this stage of oxidation, Eq. (4) gives a thickness of $\sim$0.5 Å. By way of comparison, an irradiation with 4.3×10^{13} photons cm^{-2} for 2 L of O_2 produced all oxidation states from Si^{1+} to Si^{4+} and a total thickness of 2.5 Å. Clearly, N_2O is a less efficient oxidizer of Si at 20 K during 130-eV irradiation.

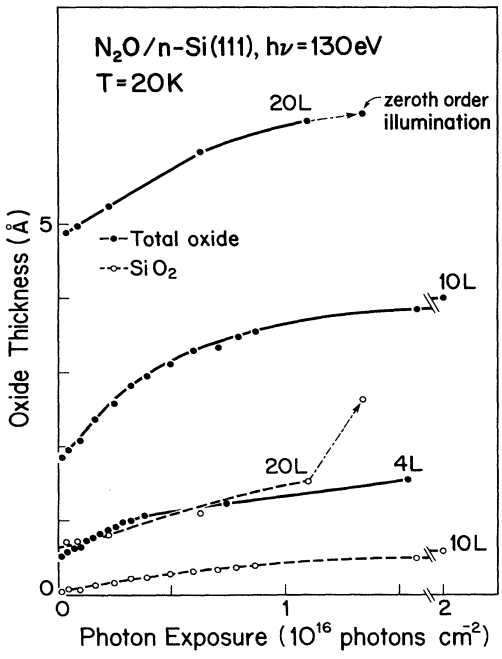

FIG. 6. Estimated oxide layer thickness as a function of photon irradiation for increased N_2O exposure. The difference between the total thickness (solid circles) and the SiO_2 thickness (open circles) is the effective thickness of the intermediate oxide. SiO_2 was not developed for 4 L N_2O exposure.

Oxidation with O_2 involves the capture of a conduction-band electron by O_2 to form reactive O_2^-. For condensed O_2, the maximum in the electron-capture cross section is below the vacuum level.[16] For gas phase N_2O, the corresponding maximum is 2.3 eV above the vacuum level.[17] Assuming that condensation of gas phase N_2O onto the surface lowers the electron affinity level in a similar fashion to O_2, then the largest cross section for condensed N_2O would still fall higher in energy than that for condensed O_2. Although 130-eV photons excite substrate electrons that can induce surface reaction for both O_2 and N_2O, the distribution of secondary electrons decreases rapidly with increased energy above the conduction-band minimum. This is one of the reasons that N_2O in contact with Si exhibits a much slower oxidation rate during initial reaction.

Figure 6 shows that the initial oxidation rate after the first illumination 4 L N_2O/Si(111) is 0.16 Å per 10^{15} photons cm^{-2}, and this rate is approximately constant until the total oxide thickness reaches $\sim$1 Å (see break in Fig. 6 for 4 L corresponding to the bottom EDC of Fig. 5). During this initial reaction stage, the intensity of the surface-shifted component decreases, and Si^{1+} is the dominant oxide species. This indicates that surface Si forms a single bond with O atoms. The oxidation rate at this stage for N_2O is $\sim$20 times slower than for O_2 after the first illumination. For oxide thickness above $\sim$1 Å, the rate is rapidly reduced to 0.04 Å per 10^{15} photons cm^{-2}, and most of the increase is due to Si^{1+} growth. The kink at $\sim$1 Å indicates the point of depletion of the available reaction sites for N_2O to be dissociated. Unless N_2 is detached from the N_2O and desorbed, the surface occupied by N_2O remains as unreactive sites. As the N_2O molecules are slowly dissociated into N_2 and O through photoillumination, O forms a bridge bond between Si atoms, i.e., Si^{1+}. During this process N_2 desorbs due to its lower condensation temperature[9] without forming Si—N bonds.[18] Further oxidation occurs at the interface between the Si substrate and the oxide layer by the diffusing O.

Comparison of photoenhanced oxidation by 4 L of N_2O with that by 2 L of O_2 (Fig. 3) shows that the oxida-

tion rate by N_2O after the first illumination ($\sim 10^{14}$ photons cm^{-2}) is ~ 20 times slower than by O_2, the oxide components consist of Si^{1+}, Si^{2+}, Si^{3+}, and Si^{4+} for O_2 but only Si^{1+} for N_2O, and the total oxide thickness is 2.5 Å for O_2 but 0.5 Å for N_2O. The oxidation rate differences originate from the difficulties of electron attachment to the condensed N_2O compared to O_2 at the first monolayer coverage, since the energy of attaching electrons to N_2O is higher and there is another barrier for escaping electrons due to trapped N_2.

The results of Fig. 6 show an increase in total oxide thickness of 0.3 Å after the first illumination of 1.0×10^{14} photons cm^{-2} for the 10 L N_2O/Si system. The increase is due primarily to Si^{1+} growth. The oxidation rate beyond the first illumination is 0.31 Å per 10^{15} photons cm^{-2}, as Si^{2+} and Si^{3+} configurations grow. Significantly, the oxidation rate behavior for 10 L N_2O was equal to that for 5 L O_2, namely an initial rate of ~ 0.3 Å per 10^{15} photons cm^{-2}, the total oxide increased by ~ 2 Å, and saturation was achieved after 7.0×10^{15} photons cm^{-2}. These similarities and differences imply that oxidation is mainly governed by the amount of O (equal amounts for O_2 and N_2O) and the thickness of the diffusion barrier (greater for O_2 than N_2O), as well as the electron-capture cross section (greater for O_2 than N_2O) after an oxide layer has been formed.

For the thicker oxides formed by condensing 10 L N_2O on the reacted surface, both Si^{2+} and Si^{3+} states are evident. Illumination by 3×10^{14} photons cm^{-2} increases the thickness by 0.9 Å and the oxidation rate thereafter is 0.19 Å per 10^{15} photons cm^{-2}. This decreased rate for larger N_2O exposure again reflects the ability of the oxide layer to act as a diffusion barrier.

Finally, comparison of the results for oxides of 6.4 Å total thickness shows that the intermediate oxides are 4.4 Å thick when formed from O_2 and 4.8 Å thick for N_2O. This indicates that the intermediate oxide formed by N_2O is somewhat broader than by O_2. We speculate that the difference is related to the single O of N_2O compared to oxidation by O_2. Subsequent zeroth-order beam illumination increases the thickness of SiO_2 by 1 Å at the expense of the intermediate oxide, equivalent to that for O_2. Again, zeroth-order illumination induces the reordering of the local structure of the formed oxide by converting intermediate oxides into more ordered SiO_2.

CONCLUSION

We have examined photoenhanced oxidation of *n*-type Si(111) at 20 K. The unity-sticking coefficient for physisorption for O_2 and N_2O at 20 K has made it possible for us to control the number of available oxygen atoms (in O_2 or N_2O) on the surface. Soft-x-ray illumination generates conduction-band electrons on Si that couple to the affinity levels of the molecules and activate both O_2 and N_2O. Detailed analysis of the Si 2*p* core-level intensities has made it possible to determine the thicknesses of the intermediate oxides and SiO_2 as a function of photon irradiation and gas exposure. Important findings include the following.

(1) SiO_2 formed at 20 K is different in local structure than that formed at elevated temperatures.

(2) The slow initial oxidation for condensed N_2O reflects the reduced electron-capture probability compared to O_2. The oxidation rate becomes similar to that of O_2 after extended illumination since the governing factor is the diffusion of O through the formed oxide.

(3) Si^{3+} is the major component of intermediate oxide formed from molecular O_2 at 20 K. This component converts to Si^{4+} with zeroth-order beam illumination or thermal annealing. The intermediate oxide formed by N_2O is broader and contains greater amounts of Si^{2+} and Si^{3+}. Continuous growth of Si^{3+} at 20 K is due to imperfections that extend throughout SiO_2. This broader intermediate oxide is formed under different conditions of O supply and kinetic constraints at 20 K.

ACKNOWLEDGMENTS

This work was supported by the Army Research Office under Contract No. DAAL03-88-K-0093. The work was performed at the Wisconsin Synchrotron Radiation Center, a facility supported by the National Science Foundation, and the assistance of its staff is gratefully appreciated.

[1]M. Tabe, T. T. Chiang, I. Lindau, and W. E. Spicer, Phys. Rev. B **34**, 2706 (1986).

[2]P. J. Grunthaner, M. H. Hecht, F. J. Grunthaner, and N. M Johnson, J. Appl. Phys. **62**, 629 (1987).

[3]A. Ourmazd, D. W. Taylor, J. A. Rentschler, and J. Bevk, Phys. Rev. Lett. **59**, 213 (1987).

[4]F. J. Himpsel, F. R. McFeely, A. Taleb-Ibrahimi, J. A. Yarmoff, and G. Hollinger, Phys. Rev. B **38**, 6084 (1988), and references therein.

[5]U. Hofer, P. Morgen, W. Wurth, and E. Umbach, Phys. Rev. B **40**, 1130 (1989).

[6]M. Nakazawa and H. Sekiyama, Appl. Phys. Lett. **56**, 2108 (1990); T. Hattori and T. Suzuki, *ibid.* **43**, 470 (1983).

[7]S. M. Goodnick, D. K. Ferry, C. W. Wilmsen, Z. Liliental, D. Fathy, and O. L. Krivanek, Phys. Rev. B **32**, 8171 (1985).

[8]H. Ibach, H. D. Bruchmann, and H. Wagner, Appl. Phys. A **29**, 113 (1982); A. J. Schell-Sorokin and J. E. Demuth, Surf. Sci. **157**, 273 (1985).

[9]J. M. Seo, S. G. Anderson, T. Komeda, C. Capasso, and J. H. Weaver, Phys. Rev. B **41**, 5455 (1990); S. G. Anderson, J. M. Seo, T. Komeda, C. Capasso, and J. H. Weaver, Appl. Phys. Lett. **56**, 2510 (1990); S. G. Anderson, T. Komeda, J. M. Seo, C. Capasso, G. D. Waddill, P. J. Benning, and J. H. Weaver, Phys. Rev. B **42**, 5082 (1990); J. M. Seo, Y. Z. Li, S. G. Anderson, D. J. W. Aastuen, U. S. Ayyala, G. H. Kroll, and J. H. Weaver, *ibid.* **42**, 9080 (1990).

[10]J. J. Joyce, M. del Giudice, and J. H. Weaver, J. Electron Spectrosc. Relat. Phenom. **49**, 31 (1989).

[11]I. M. Vitomirov, C. M. Aldao, G. D. Waddill, and J. H. Weaver, J. Vac. Sci. Technol. A **8**, 3368 (1990).

[12]F. J. Grunthaner, P. J. Grunthaner, R. P. Vasquez, B. F. Lewis, J. Maserjian, and A. Madhukar, Phys. Rev. Lett. **43**,

1683 (1979).
[13]R. L. Mozzi and B. E. Warren, J. Appl. Cryst. **2**, 164 (1969).
[14]J. E. Demuth, W. J. Thomson, N. J. DiNardo, and R. Imbihl, Phys. Rev. Lett. **56**, 1408 (1986).
[15]K. A. Bertness, T. T. Chiang, C. E. McCants, P. H. Mahowald, A. K. Wahi, T. Kendelewicz, I. Lindau, and W. E. Spicer, Surf. Sci. **185**, 544 (1987).
[16]L. Sanche and M. Deschenes, Phys. Rev. Lett. **61**, 2096 (1988).
[17]D. Rapp and D. D. Briglia, J. Chem. Phys. **43**, 1480 (1965).
[18]E. G. Keim and A. Van Silfhout, Surf. Sci. **152/153**, 1096 (1985); E. G. Keim, L. Wolterbeek, and A. Van Silfhout, *ibid.* **180**, 565 (1987); K. A. Bertness, P. H. Mahowald, C. E. McCants, A. K. Wahi, T. Kendelewicz, I. Lindau, and W. E. Spicer, Appl Phys. A **47**, 219 (1988); E. G. Keim, H. Wormeester, and A. Van Silfhout, J. Vac. Sci. Technol. A **8**, 2747 (1990).